Chiral Ions in the Gas Phase. 1. Intramolecular Racemization and Isomerization of O-Protonated (*S*)-*trans*-4-Hexen-3-ol

Anna Troiani,[†] Francesco Gasparrini,[†] Felice Grandinetti,[‡] and Maurizio Speranza*,[†]

Contribution from the Facoltà di Farmacia, Dipartimento di Studi di Chimica e Tecnologia delle Sostanze Biologicamente Attive, Università degli Studi di Roma "La Sapienza", P.le A. Moro 5, 00185 Rome, Italy, and the Dipartimento di Scienze Ambientali, Università della Tuscia, Viterbo, Italy

Received January 22, 1996[⊗]

Abstract: The acid-catalyzed racemization and regioisomerization of (*S*)-*trans*-4-hexen-3-ol (**1S**) has been investigated in gaseous CH_4 and C_3H_8 at 720 Torr and in the 40−120 °C temperature range. The contribution to the racemization and isomerization products by free 1-methyl-3-ethylallyl cations, arising from unimolecular fragmentation of excited O-protonated (*S*)-*trans*-4-hexen-3-ol (**IS**), was evaluated by generating them from protonation of isomeric 2,4-hexadienes and by investigating their behavior toward $H_2{}^{18}O$ under the same experimental conditions. The rate constant of the gas phase racemization of **IS** ($1.4-21.3 \times 10^6$ s^{-1}) was found to exceed that of its isomerization ($1.0-9.9 \times 10^6$ s^{-1}) over the entire temperature range. The experimental results, combined with *ab initio* theoretical calculations on the model [$C_3H_5{}^+/H_2O$] system, are consistent with a gas phase intramolecular **IS** racemization and isomerization involving the intermediacy of structured ion−molecule complexes, wherein the H_2O molecule is coplanarly coordinated to the hydrogen atoms of the 1-methyl-3-ethylallyl moiety. The rate of formation of these structured complexes, their relative stability, and the dynamics of their evolution to the racemized and isomerized products depend, in the gas phase, on the specific conformation of **IS**. The relevant activation parameters point to transition structures wherein a substantial fraction of the positive charge is located on the allyl moiety. The results obtained in the present gas phase investigation confirm previous indications about the occurrence and the role of intimate ion−molecule pairs in acid-catalyzed racemization and isomerization of optically active alcohols, including allylic alcohols, in solution.

Introduction

Despite the recent development of novel approaches for chiral recognition by mass spectrometric methods,[1] the study of gas phase reactions involving optically active ions with a single chiral center still remains a virtually unexplored facet of the gas phase ion chemistry field.[2] The present investigation is a first attempt to fill this gap, the emphasis being on the kinetics and the dynamics of intramolecular rearrangements in chiral oxonium ions.

The study was stimulated from a recent gas phase investigation of the mechanism of acid-induced nucleophilic substitution on some allylic alcohols using radiolytic methods.[3] It was demonstrated that the reaction proceeds through the concerted S_N2' pathway (eq ii of Scheme 1), in competition with the classical S_N2 one (eq i of Scheme 1). Unequivocal evidence for these mechanisms was achieved only after careful weighing of the unimolecular processes which normally accompany bimolecular allylic substitution in solution,[4] namely unimolecular dissociation (S_N1, eq iii of Scheme 1) and intramolecular isomerization of the involved allylic oxonium intermediates (S_Ni', eq iv of Scheme 1). For instance, in 760 Torr of CH_4 at 37.5 °C, up to 12% of intramolecular interconversion (eq iv of Scheme 1) was observed in the oxonium intermediates with R/R′ = H/Me, *trans*-Me/H, and *cis*-Me/H prior to substitution by methanol.[3a,b] Under the same conditions, 11% is the maximum extent of interconversion observed prior to nucleophilic attack in the fraction (≥81%) of oxonium intermediates from protonation of 1-methyl-2-cyclohexen-1-ol and 3-methyl-2-cyclohexen-1-ol surviving unimolecular fragmentation.[3c]

The natural continuation of this study is the assessment of the intrinsic stereochemistry of the bimolecular reactions i and ii of Scheme 1 in the gas phase (i.e., without interference from solvation and ion-pairing effects) and its comparison with theoretical predictions which normally refer to isolated species. The use of chiral oxonium ions and the unequivocal definition of their structure immediately before bimolecular substitution are required to achieve this goal. The present study addresses this latter point by analyzing the kinetics and the mechanisms of unimolecular isomerization and racemization of a model chiral oxonium ion under typical gas phase nucleophilic substitution conditions.

[†] Università degli Studi di Roma "La Sapienza".

[‡] Università della Tuscia.

[⊗] Abstract published in *Advance ACS Abstracts,* April 15, 1997.

(1) Sawada, M.; Takai, Y.; Yamada, H.; Hirayama, S.; Kaneda, T.; Tanaka, T.; Kamada, K.; Mizooku, T.; Takeuchi, S.; Ueno, K.; Hirose, K.; Tobe, Y.; Naemura, K. *J. Am. Chem. Soc.* **1995**, *117*, 7726 and references therein.

(2) An outstanding exception is provided: Hall, D. G.; Gupta, C.; Morton, T. H. *J. Am. Chem. Soc.* **1981**, *103*, 2416.

(3) (a) Dezi, E.; Lombardozzi, A.; Pizzabiocca, A.; Renzi, G.; Speranza, M. *J. Chem. Soc., Chem. Commun.* **1995**, 547. (b) Renzi, G.; Lombardozzi, A.; Dezi, E.; Pizzabiocca, A.; Speranza, M. *Chem. Eur. J.* **1996**, *2*, 316. (c) Dezi, E.; Lombardozzi, A.; Renzi, G.; Pizzabiocca, A.; Speranza, M. *Chem. Eur. J.* **1996**, *2*, 323.

(4) (a) DeWolfe, R. H.; Young, W. G. *Chem. Rev.* **1956**, *56*, 753. (b) Bordwell, F. G. *Acc. Chem. Res.* **1970**, *3*, 281. (c) McLennan, D. J. *Acc. Chem. Res.* **1976**, *9*, 281. (d) Magid, R. M. *Tetrahedron* **1980**, *36*, 1901. (e) Young, W. G.; Winstein, S.; Goering, H. L. *J. Am. Chem. Soc.* **1951**, *73*, 1958. (f) D'Incan, E.; Viout, P. *Bull. Soc. Chim. Fr.* **1971**, *9*, 3312. (g) Meislich, H.; Jasne, S. J. *J. Org. Chem.* **1982**, *47*, 2517. (h) Kepner, R. D.; Winstein, S.; Young, W. G. *J. Am. Chem. Soc.* **1949**, *71*, 115.

S0002-7863(96)00212-0 CCC: $14.00

Scheme 1

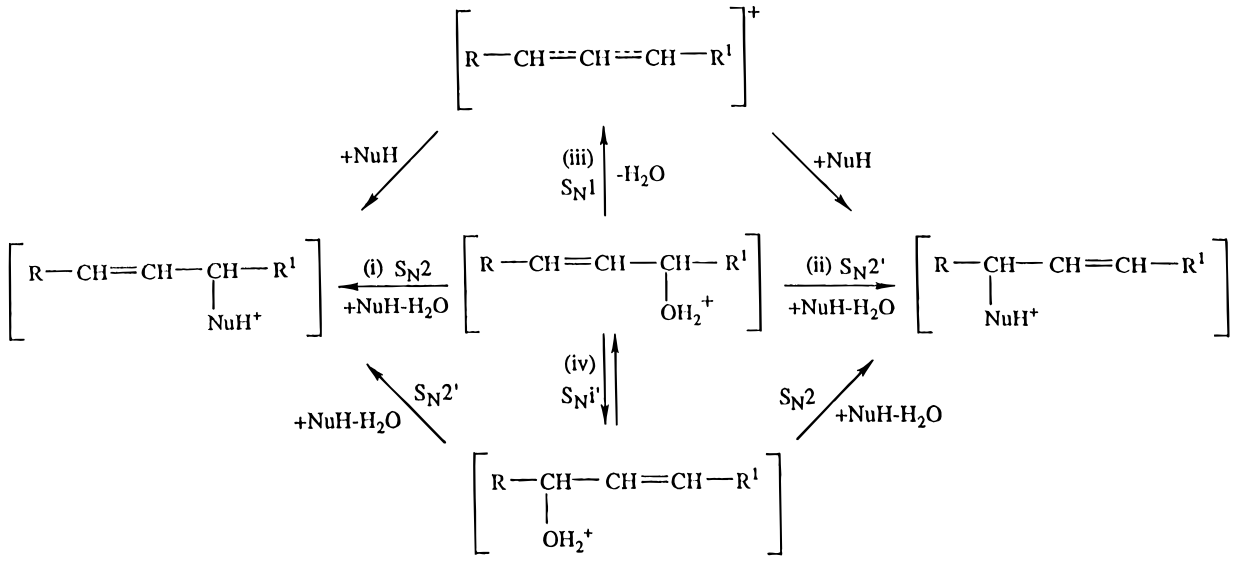

Scheme 2

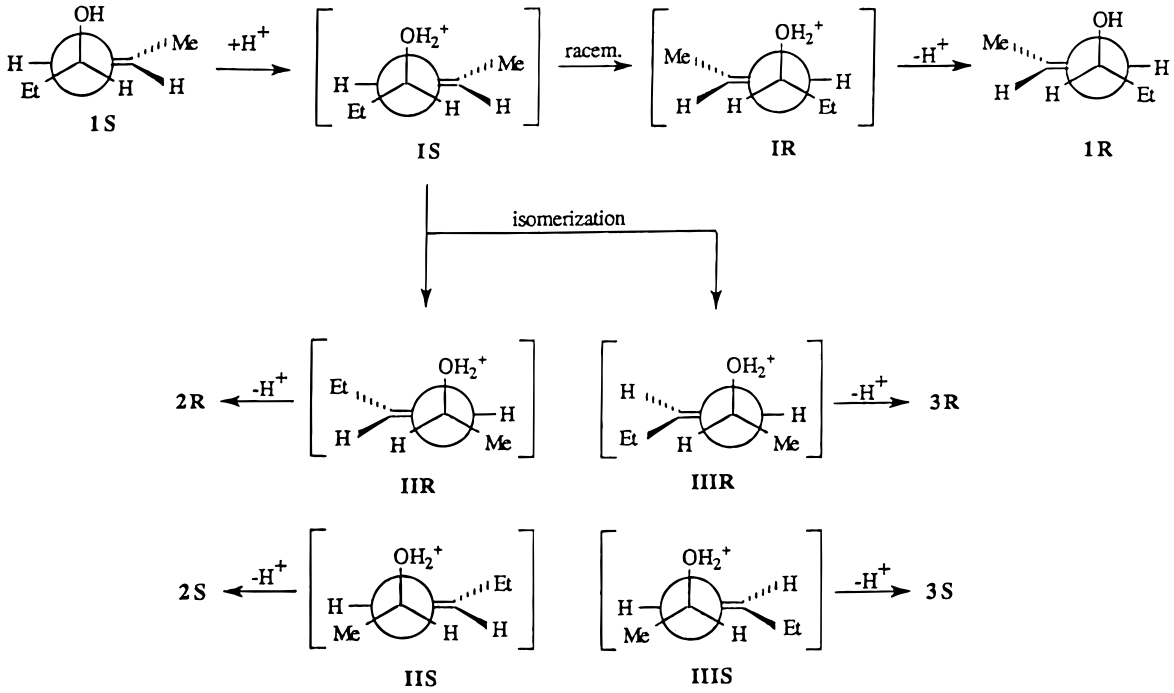

The selected chiral oxonium ion was **IS** (Scheme 2), obtained in the gas phase from O-protonation of the *S*-enantiomer of *trans*-4-hexen-3-ol (**1S**). To this purpose, stationary concentrations of the protonating agents have been generated from γ-radiolysis of gaseous mixtures, containing either CH_4 or C_3H_8 as the bulk component (720 Torr), together with traces of the chiral alcohol **1S** (0.7−1.0 Torr), of O_2 as a radical scavenger (10 Torr), and of $(MeO)_3PO$ as a base (0.5−0.9 Torr) with a proton affinity (PA) of 212.0 kcal mol^{-1}.[5] Under such conditions, the high collisional frequency (ca. 10^{10} s^{-1}) with the bulk gas molecules favors stabilization and thermal equilibration of **IS** prior to its rearrangement, whose course is inferred from the yield and composition of the neutral rearranged products (i.e., **1R**, **2R**, **2S**, **3R**, and **3S** (Scheme 2)), formed by neutralization of their ionic precursors (i.e., **IR**, **IIR**, **IIS**, **IIIR**, and **IIIS**) with the base $(MeO)_3PO$.

It is hoped that this study, which represents the first kinetic and mechanistic investigation on optically active cations in the gas phase, may provide kinetic information upon the unimolecular rearrangement of the free, unsolvated oxonium intermediate **IS**, as well as on the dynamics of the H_2O molecule moving around the allyl ion backbone as a function of the conformation of the rearranging species. Moreover, a comparison of the gas phase results with those from analogous solvolytic studies may contribute to unravelling the role of intimate ion−molecule pairs in the racemization and isomerization of optically active alcohols and ethers in acidic solutions.[6−15]

(5) Lias, S. G.; Bartmess, J. E.; Liebman, J. F.; Holmes, J. L.; Levin, R. D.; Mallard, W. G. *J. Phys. Chem. Ref. Data* **1988**, *17*, Suppl. 1.

(6) For reviews, see: (a) Samuel, D.; Silver, B. *Adv. Phys. Org. Chem.* **1965**, *3*, 128. (b) Raber, D. J.; Harris, J. M.; Schleyer, P. v. R. *Ions and Ion Pairs in Organic Reactions* Szwarc, M., Ed.; Wiley: New York, 1974; Vol. 2.

(7) Herlihy, K. P. *Aust. J. Chem.* **1982**, *35*, 2221.

(8) Allen, A. D.; Kanagasabapathy, V. D.; Tidwell, T. T. *J. Am. Chem. Soc.* **1984**, *106*, 1361.

(9) Dietze, P. E.; Jencks, W. P. *J. Am. Chem. Soc.* **1987**, *109*, 2057.

Experimental Section

Materials. Methane, propane, and oxygen were high-purity gases from Matheson Co. and used without further purification. $H_2{}^{18}O$ (^{18}O-content > 97%), $(MeO)_3PO$, triethylamine, *trans*,*trans*-2,4-, *cis*,*trans*-2,4-, and *trans*-1,3-hexadiene were research grade chemicals from Aldrich Chemical Co. The racemate of (*S*,*R*)-*trans*-4-hexen-3-ol (henceforth denoted by **1S**-**1R**) and (*S*,*R*)-*trans*-3-hexen-2-ol (henceforth denoted by **2S**-**2R**) were prepared according to well-established procedures[16] and purified by semipreparative HPLC on a LiChrosorb Si-60 column, 5 μm, 250 × 10 mm i.d., eluent 85/15 (v/v) = hexane/ethyl acetate, flow rate 5.0 mL min^{-1}, detection by refractive index, retention factors $k'_{(\mathbf{1}-\text{ester})} \approx k'_{(\mathbf{2}-\text{ester})} = 0.33$ and $k'_{(\mathbf{1}-\text{alcohol})} \approx k'_{(\mathbf{2}-\text{alcohol})} = 2.46$.

Kinetic resolution of the **1S**-**1R** and **2S**-**2R** racemates was carried out by enantioselective biotransformations according to the following procedure. Lipase (54 mg) from *Pseudomonas* species type XIII (Sigma Chemical Co.), supported on a modified silica matrix,[17] was added to a magnetically stirred solution of **1S**-**1R** (or **2S**-**2R**) (300 mg, 3 mmol) and acetic anhydride (0.423 mL, 4.5 mmol) in benzene (7.5 mL). The reaction mixture was stirred at room temperature. Periodically, 0.5 μL aliquots of the liquid phase were withdrawn and analyzed by GLC to follow the progress of the reaction. After 24 h, approximately 50% conversion of the alcohol in acetic ester was reached, and the reaction was stopped. The enzymic suspension was filtered, and the filtrate was evaporated to dryness. The residue, consisting of the *S*-enantiomer of the starting alcohol **1S** (or **2S**) and the acetic ester of the *R*-enantiomer of the starting alcohol **1R** (or **2R**), was recovered. The *R*-ester was then separated from the *S*-alcohol by semipreparative HPLC on the LiChrosorb Si-60 column, under the conditions described above. The enantiomeric excess (ee) of the purified (*S*)-*trans*-4-hexen-3-ol (**1S**) (or (*S*)-*trans*-3-hexen-2-ol (**2S**)) was 98.5%, as determined by chiral capillary GLC (25 m long, 0.25 mm i.d. MEGADEX 5 (30% dimethylpentyl-β-cyclodextrin in OV 1701) fused silica column, operated at temperatures ranging from 50 to 80 °C, 3 °C min^{-1}).

The residue, containing the acetic ester of *R*-enantiomer of *trans*-4-hexen-3-ol (**1R)** (or *trans*-3-hexen-2-ol (**2R**)), was dissolved in 95/5 (v/v) = water/acetone solution (5 mL) containing 0.18 mL of 0.3 N NaOH. The solution was stirred at room temperature for 20 h and periodically analyzed by GLC. After the hydrolysis was completed, the solvent was evaporated and the residue was purified by semi-preparative HPLC on the LiChrosorb Si-60 column, under the conditions described above. The ee of the purified **1R** (or **2R**) was 99.0%, as determined by chiral capillary GLC.

Procedure. The gaseous mixtures were prepared by introducing fragile ampules, containing weighed amounts of the chiral alcohol **1S**, into carefully outgassed 135 mL Pyrex bulbs, equipped with a break-seal tip and connected to a greaseless vacuum line. Following the introduction of the other gaseous components at the desired partial pressures, the bulbs were cooled to the liquid nitrogen temperature and sealed off. The fragile ampules were then broken, and the gaseous components were allowed to mix before being irradiated. The irradiations were carried out at a temperature ranging from 40 to 120 °C in a 220 Gammacell from Nuclear Canada Ltd. to a dose of 2 × 10^4 Gy at a rate of 10^4 Gy h^{-1}, as determined by a neopentane dosimeter. Control experiments, carried out at doses ranging from 1 × 10^4 to 1 × 10^5 Gy, showed that the relative yields of products are largely independent of the dose. The radiolytic products were analyzed by GLC, using a Perkin-Elmer 8700 gas chromatograph equipped with a flame ionization detector (FID), on the 25 m long, 0.25 mm i.d. MEGADEX 5 fused silica column, operated at the same conditions as reported above. The products were identified by comparison of their retention volumes with those of authentic standard compounds, and their identity confirmed by GLC-MS, using a Hewlett-Packard 5890 A gas chomatograph in line with a HP 5970 B mass selective detector. Their yields were determined from the areas of the corresponding eluted peaks, using the internal standard (i.e., 3-methylpentan-3-ol) method and individual calibration factors to correct for the detector response. Blank experiments were carried out to ascertain the occurrence and the extent of thermal isomerization and racemization of **1S** at any given reaction temperature. The yields of the radiolytic products from gas phase protonation of **1S** were corrected accordingly.

Computational Details. The *ab initio* calculations were performed using a IBM RISC/6000 version of the Gaussian 92[18a] and Gaussian 94[18b] sets of programs. The geometries of the investigated species were optimized at the MP2(full)/6-31G* level of theory, and their real character on the surface (minimum, transition structure, higher-order saddle point) ascertained by computing the corresponding analytical vibrational frequencies. In particular, the transition structures connecting selected energy minima along the appropriate reaction paths were located using the synchronous transit-guided quasi-Newton method implemented by Schlegel and co-workers,[18c] available as a standard routine (QST3) in Gaussian 94. In addition, the zero-point energies (ZPEs) of all of the investigated species were calculated using the MP2-(full)/6-31G* vibrational frequencies. Finally, single-point calculations at the MP4/6-311G** and QCISD(T)/6-311G** computational levels were performed in correspondence of the MP2 geometries to better estimate the influence of the correlation energy on the relative stability of the various $[C_3H_5{}^+/H_2O]$ structures.

Results

Radiolytic Experiments. Table 1 reports the composition of the irradiated mixtures and the absolute yields of the products formed from the gas phase protonation of **1S**, in the presence of the base (B = $(MeO)_3PO$). The absolute yields of the products are given as G(M) values, defined as the number of molecules of product M formed per 100 eV of absorbed energy. The product pattern is characterized by the formation of the enantiomer **1R** of the starting substrate, accompanied by the racemate of their *trans*-isomer **2R**-**2S**, in proportions depending upon the experimental conditions. No formation of the *cis*-enantiomers **3R** and **3S** is observed under the same conditions (G(M) < 0.001). The *cis*,*trans*-2,4-, *trans*,*trans*-2,4-, and *trans*-1,3-hexadiene ("dienes" in Table 1) are also major products with an overall yield increasing with the temperature. In the systems with C_3H_8 as the bulk gas, these products are accompanied by the formation of *trans*-3-isopropoxy-4-hexenes and *trans*-2-isopropoxy-3-hexenes, in yields independent of temperature (Table 1).

Ancillary experiments have been carried out under the same conditions of Table 1 to verify the tendency of free 1-methyl-3-ethylallyl cations to add water, yielding **1R**, **1S**, **2R**, **2S**, **3R**, and **3S**. Free *exo*-1-methyl-*exo*-3-ethylallyl cations have been generated in 720 Torr of bulk gas at 40−120 °C by radiolytic protonation of *trans*,*trans*- or *cis*,*trans*-2,4-hexadiene (0.5−1.3 Torr) in the presence of ca. 2 Torr of $H_2{}^{18}O$ (^{18}O-content > 97%) (Table 2). These free allyl cations were found to add to

(10) Merritt, M. V.; Bronson, G. E.; Baczynskyj, L.; Boal, J. R. *J. Am. Chem. Soc.* **1980**, *102*, 346.
(11) Merritt, M. V.; Bell, S. J.; Cheon, H. J.; Darlington, J. A.; Dugger, T. L.; Elliott, N. B.; Fairbrother, G. L.; Melendez, C. S.; Smith, E. V.; Schwartz, P. L. *J. Am. Chem. Soc.* **1990**, *112*, 3560.
(12) Merritt, M. V.; Anderson, D. B.; Basu, K. A.; Chang, I. W.; Cheon, H. J.; Mukundan, N. E.; Flannery, C. A.; Kim, A. Y.; Vaishampayan, A.; Yens, D. A. *J. Am. Chem. Soc.* **1994**, *116*, 5551.
(13) Thibblin, A. *J. Chem. Soc., Perkin Trans. 2* **1987**, 1987.
(14) Thibblin, A. *J. Chem. Soc., Chem. Commun.* **1990**, 697.
(15) Thibblin, A. *J. Chem. Soc., Perkin Trans. 2* **1992**, 1195.
(16) Coburn, E. R. *Organic Syntheses*; Wiley: New York, 1995; Collect. Vol. 3, p 696.
(17) Cernia, E.; Palocci, C.; Gasparrini, F.; Misiti, D.; Fagnano, N. *J. Mol. Catal.* **1994**, *89*, L11.
(18) (a) GAUSSIAN 92, Revision A; Frish, M. J.; Trucks, G. W.; Head-Gordon, M.; Gill, P. M. W.; Wong, M. W.; Foresman, J. B.; Johnson, B. G.; Schlegel, H. B.; Robb, M. A.; Repogle, E. S.; Gomperts, R.; Andres, J. L.; Ragavachari, K.; Binkley, J. S.; Gonzales, C.; Martin, R. L.; Fox, D. J.; Defrees, D. J.; Baker, J.; Stewart, J. J. P.; Pople, J. A.; Gaussian, Inc.: Pittsburgh, PA, 1992. (b) GAUSSIAN 94, Revision C.2; Frish, M. J.; Trucks, G. W.; Schlegel, H. B.; Gill, P. M. W.; Johnson, B. G.; Robb, M. A.; Cheeseman, J. R.; Keith, T. A.; Petersson, G. A.; Montgomery, J. A.; Ragavachari, K.; Al-Laham, M. A.; Zakrzewski, V. G.; Ortiz, J. V.; Foresman, J. B.; Cioslowski, J.; Stefanov, B. B.; Nanayakkara, A.; Challacombe, M.; Peng, C. Y.; Ayala, P. Y.; Chen, W.; Wong, M. W.; Andres, J. L.; Repogle, E. S.; Gomperts, R.; Martin, R. L.; Fox, D. J.; Binkley, J. S.; Defrees, D. J.; Baker, J.; Stewart, J. J. P.; Head-Gordon, M.; Gonzales, C.; Pople, J. A.; Gaussian, Inc.: Pittsburgh, PA, 1995. (c) Peng, C.; Schlegel, H. B. *Isr. J. Chem.* **1993**, *33*, 449.

Table 1. Absolute Yields of the Products from the Gas Phase Protonation of **1S** in the presence of $(MeO)_3PO$

system composition[a]			reactn temp	absolute product yields, G(M)[b]				
				G(**2R-2S**)				
bulk gas	**1S** (Torr)	$(MeO)_3PO$ (Torr)	(°C)	G(**1R**)	G(**2R**)	G(**2S**)	G(**dienes**)[c]	G(**ethers**)[d]
CH_4	0.69	0.53	40	0.060	0.025	0.027	0.302	
CH_4	0.84	0.88	70	0.153	0.053	0.053	0.520	
CH_4	1.05	0.84	100	0.175	0.067	0.068	0.809	
CH_4	0.84	0.88	120	0.065	0.016	0.018	0.985	
C_3H_8	0.70	0.62	40	0.085	0.037	0.036	0.090	0.215
C_3H_8	0.76	0.64	100	0.110	0.037	0.037	0.890	0.215

[a] Bulk gas: 720 Torr. O_2 : 4 Torr. Radiation dose 2×10^4 Gy (dose rate: 1×10^4 Gy h^{-1}). [b] G(M) as the number of molecules M produced per 100 eV of absorbed energy. Each value is the average of several determinations, with an uncertainty level of ca. 5%. [c] Combined yields of *trans*,*trans*-2,4-, *cis*,*trans*-2,4-, and *trans*-1,3-hexadiene. [d] Combined yields of *trans*-3-isopropoxy-4-hexene and *trans*-2-isopropoxy-3-hexene.

Table 2. Absolute Yields and ^{18}O-Content of Allylic Alcohols from Protonation of Isomeric 2,4-Hexadienes in the Presence of $H_2{}^{18}O$

system composition[a]			reactn temp	overall absolute yield,	^{18}O-content, (%)[d]	
bulk gas	2,4-hexadiene (Torr)[b]	$H_2{}^{18}O$ (Torr)	(°C)	G(M)[c]	**1R-1S**	**2R-2S**
CH_4	0.63 (0.65)	2.0 (1.9)	40	0.30 (0.32)	53 (54)	52 (55)
CH_4	0.60 (0.59)	2.0 (1.8)	70	0.12 (0.14)	54 (54)	54 (52)
CH_4	0.53 (0.58)	1.9 (2.1)	100	0.05 (0.04)	54 (55)	55 (53)
CH_4	0.68 (0.73)	2.1 (2.0)	120	<0.001 (<0.001)	n.d. (n.d.)[e]	n.d. (n.d.)[e]
C_3H_8	1.26 (1.05)	2.7 (2.5)	40	0.21 (0.24)	35 (36)	40 (40)
C_3H_8	1.10 (0.96)	2.4 (2.2)	100	0.04 (0.04)	38 (37)	40 (41)

[a] Bulk gas: 720 Torr. O_2: 4 Torr. Radiation dose 2×10^4 Gy (dose rate: 1×10^4 Gy h^{-1}). [b] The *trans*,*trans*-isomer. The results concerning experiments with *cis*,*trans*-isomer are given in parentheses. [c] See footnote *b* in Table 1. [d] Uncertainty level, ca. 5%. [e] n.d. = below detection limit (ca. 2%).

Table 3. Absolute Yields and ^{18}O-Content of Allylic Alcohols from Protonation of **1S** in the Presence of $H_2{}^{18}O$

system composition[a]			reactn temp	absolute yields[b]		overall product yield,	^{18}O-content (%)[c]	
bulk gas	**1S** (Torr)	$H_2{}^{18}O$ (Torr)	(°C)	G(**1R**)	G(**2R-2S**)	G(M)[b]	**1R**	**2R-2S**
CH_4	0.63	2.0	40	0.04	0.05	0.09	18	25
CH_4	0.67	2.1	70	0.04	0.06	0.10	17	24
CH_4	0.53	2.0	100	0.11	0.09	0.20	13	23
CH_4	0.58	2.0	120	0.06	0.04	0.10	n.d.[d]	n.d.[d]
C_3H_8	0.62	2.0	40	0.05	0.06	0.11	16	23
C_3H_8	0.63	1.8	100	0.07	0.07	0.14	4	9

[a] Bulk gas: 720 Torr. O_2: 4 Torr. Radiation dose 2×10^4 Gy (dose rate: 1×10^4 Gy h^{-1}). [b] See footnote *b* in Table 1. [c] Uncertainty leve, ca. 5%. [d] n.d. = below detection limit (ca. 2%).

$H_2{}^{18}O$ yielding equal amounts of **1S**-**1R** and **2S**-**2R**, in absolute yields decreasing by increasing the temperature, and again, no formation of the *cis*-enantiomers **3R** and **3S** was observed. The overall G(M) values of **1S**-**1R** and **2S**-**2R**, measured in these systems, range from 0.3 at 40 °C to <0.001 at 120 °C. The ^{18}O-content in these products, as determined by mass spectrometry from the relative abundances of their $[M - 29]^+$ (m/z = 71(^{16}O); 73(^{18}O)) and $[M - 15]^+$ (m/z = 85(^{16}O); 87(^{18}O)) fragments, amounts to 54 ± 2% in CH_4 and 38 ± 3% in C_3H_8 and appears essentially independent of temperature (last two columns of Table 2). In a similar set of experiments with $H_2{}^{18}O$ (^{18}O-content > 97%) carried out with **1S** instead of a 2,4-hexadiene as the starting substrate, the **1R** and **2S**-**2R** alcohols were obtained as well, in yields displaying no monotonic dependence with temperature (Table 3). Their ^{18}O-content is appreciably lower than that of the same products from the corresponding experiments with *exo*-1-methyl-*exo*-3-ethylallyl cations and is found to decrease monotonically by increasing the reaction temperature (Table 3).

Theoretical Calculations. The structure, the stability, and the interconversion processes of several $[C_3H_5{}^+/H_2O]$ adducts have been investigated by *ab initio* theoretical calculations at the post-SCF level of theory. Exploration of the MP2(full)/6-31/G* potential energy surface of $[C_3H_5{}^+/H_2O]$ around different conceivable regions led to the location of seven different critical points, unambiguously characterized as true minima or transition structures by analytical computation of the corresponding vibrational frequencies. The connectivity and the main geometrical parameters of these ions are shown in Figure 1 and their absolute and relative energies, at the various computational levels, are collected in Table 4.

As a general observation, the MP2(full)/6-31G* relative stability of the investigated $[C_3H_5{}^+/H_2O]$ structures is only modestly affected at the MP4/6-311G**//MP2/6-31G* computational level and does not change appreciably by upgrading the calculation at the QCISD(T)/6-311G**//MP2/6-31G* level. Thus, only the values obtained at this latter computational level will be discussed.

Ion **A**, formally obtained by interacting a water molecule with the carbon atom of one of the CH_2 moieties of a free allyl cation, is the most stable among the investigated $[C_3H_5{}^+/H_2O]$ structures. Its optimized geometrical parameters (Figure 1a) suggest a significant interaction between $C_3H_5{}^+$ and H_2O. The C−O bond distance (1.575 Å) is only slightly longer than the carbon−oxygen bond in $CH_3OH_2{}^+$ (i.e., 1.516 Å). The C1 possesses a significant degree of pyramidalization, as suggested by the O−C1−C2 (105.9°) and H1−C1−H2 (112.4°) bond angles (cf., this latter value with the H1−C1−H2 angle of 117.2° in the free allyl cation **D** (Figure 1d)). In addition, the interaction between $C_3H_5{}^+$ and H_2O significantly perturbs the π-system of the free $C_3H_5{}^+$ ion **D**, whose C1−C2 and C2−C3 bond distances (1.382 Å) become 1.470 and 1.343 Å, respectively, in ion **A**. These variations are consistent with a high degree of localization of the π-bond between C2 and C3. Adding the thermal contribution (300 K) to the total energies reported in Table 4, the enthalpy change for the dissociation of ion **A** into $C_3H_5{}^+$ and H_2O is evaluated to be as large as 26 kcal mol^{-1}, in excellent agreement with previous *ab initio* estimates.[19] Combining this

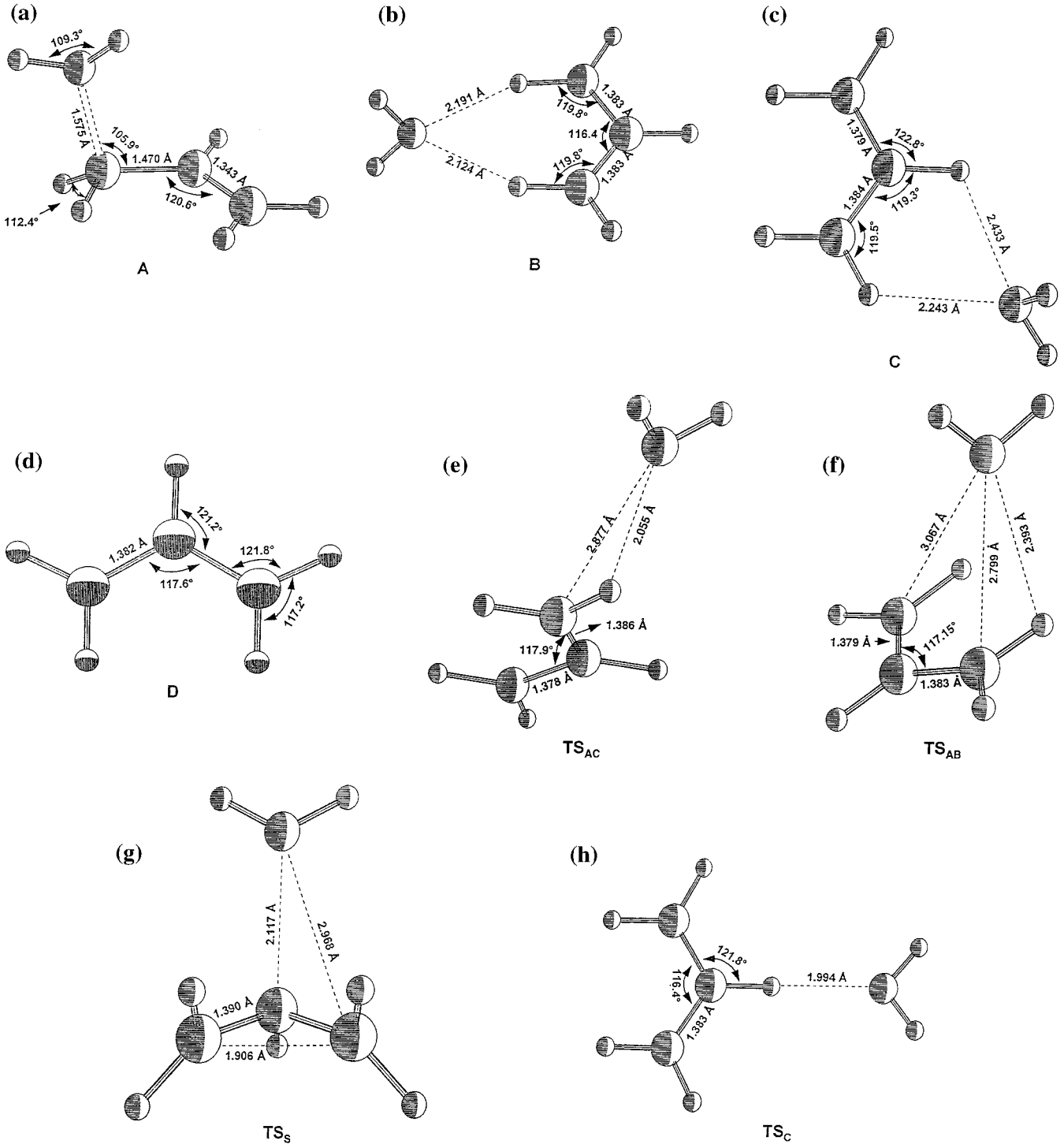

Figure 1. MP2(full)/6-31G*-optimized geometries of the investigated [$C_3H_5^+/H_2O$] system: (a) global minimum **A**; (b) local minimum **B**; (c) local minimum **C**; (d) allyl cation **D**; (e) first-order saddle point $\mathbf{TS_{AC}}$; (f) first-order saddle point $\mathbf{TS_{AB}}$; (g) first-order saddle point $\mathbf{TS_S}$; (h) first-order saddle point $\mathbf{TS_C}$. Bond lengths are in angstrom, and bond angles are in degrees.

computed binding energy with the experimental heats of formation of the allyl cation (226.0 kcal mol^{-1})[5] and of H_2O ($-$57.8 kcal mol^{-1}),[5] a *theoretical* heat of formation of 142 kcal mol^{-1} is estimated for ion **A**.

Two additional [$C_3H_5^+/H_2O$] energy minima, henceforth denoted as **B** and **C**, have been located on the MP2/6-31G* potential energy surface (Figure 1b,c). From Table 4, they are less stable than **A** by 8.3 and 10.5 kcal mol^{-1}, respectively, and their dissociation enthalpies into $C_3H_5^+$ and H_2O (i.e., 15.3 and 13.1 kcal mol^{-1}, respectively) decrease accordingly. The optimized geometrical parameters of **B** and **C** are consistent with those of structured ion$-$dipole complexes between $C_3H_5^+$ and H_2O, held together by hydrogen-bond-like electrostatic interactions, with no appreciable covalent bonding between the two interacting moieties. In the C_1-symmetric structure **B** (Figure 1b), this is demonstrated by the rather long O$-$H1 (2.191 Å) and O$-$H5 (2.124 Å) bond distances and by the observation that the geometrical parameters of the C_3H_5 moiety do not change appreciably relative to those of free $C_3H_5^+$ ion **D** (Figure 1d). We note here that the conceivable existence of C_{2v}-symmetric structures close to **B** was checked by imposing the proper symmetry constraints in the geometry optimization. A novel fully planar critical point was actually located, but characterized as a first-order saddle point, unstable with respect

(19) Nobes, R. H.; Radom, L. *Org. Mass Spectrom.* **1984**, *19*, 385.

Table 4. Computed MP2, MP4, and QCI Absolute (au) and Relative Energies (kcal mol^{-1}, including ZPEs) and Zero-Point Energies (ZPE, kcal mol^{-1}) of [$C_3H_5^+$/H_2O] Structures

structure	MP2	ZPE	MP4	QCI	ΔE(MP2)	ΔE(MP4)	ΔE(QCI)	S(eu)
A	−192.80441	62.2	−192.98609	−192.98731	0.0	0.0	0.0	70.8
B	−192.78504	59.6	−192.96860	−192.96986	+10.6	+8.4	+8.3	78.4
C	−192.78064	59.1	−192.96433	−192.96557	+11.7	+10.6	+10.5	80.7
TS_{AC}	−192.77788	58.7	−192.96155	−192.96286	+13.1	+11.9	+11.8	80.5
TS_{AB}	−192.77988	59.0	−192.96341	−192.96479	+12.2	+11.0	+10.9	77.2
TS_S	−192.76217	59.2	−192.94351	−192.94393	+23.5	+23.7	+24.2	74.0
TS_C	−192.77821	58.9	−192.96162	−192.96283	+13.1	+12.0	+12.1	76.8
D	−116.55762	43.9	−116.66487	−116.66602	+25.0	+23.5	+23.6	
H_2O	−76.19924	13.5	−76.27607	−76.27607				

to the out-of-plane rotation of the H atoms of water. Ion **C** (Figure 1c) formally arises by interacting a water molecule with the H2 and H3 atoms of the free allyl cation. The O−H2 (2.243 Å) and O−H3 (2.433 Å) bond distances are comparatively greater than those of structure **B** (2.124−2.192 Å), thus suggesting relatively weaker interactions, that with H2 being more intense than that with H3. Consistently, the variation of the H2−C1−C2 bond angle (119.5°), relative to that of the free $C_3H_5^+$ ion **D** (121.8°; Figure 1d), is more pronounced than that of the H3−C2−C1 one (119.3° vs 121.2°). Finally, we note here that, despite careful searching around this region of the MP2/6-31G* potential energy surface, no energy minima were located with the water molecule coordinated between the H1 and H2 centers of the allylic moiety, thus pointing to unfavorable energy requirements for four-center arrangements.

The search of transition structures connecting the above energy minima led to four distinct first-order saddle points (i.e., **TS_{AC}**, **TS_{AB}**, **TS_S**, and **TS_C** (Figure 1e−h)). The transition structure **TS_{AC}** (imaginary frequency 97.1*i* cm^{-1}) connects ion **A** with intermediate **C** and lies 11.8 kcal mol^{-1} above **A**. The structure of **TS_{AC}** indicates that the **A** → **C** rearrangement is allowed only after a substantial elongation of the C1−O bond from 1.575 Å (**A**, Figure 1a) to 2.877 Å (**TS_{AC}**, Figure 1e). Consistently, in **TS_{AC}**, the C−C bond distances of the allylic moiety (1.386 (C1−C2) and 1.378 Å (C2−C3)) are only slightly different from those of free $C_3H_5^+$ ion **D** (1.382 Å, Figure 1d), while diverging substantially from the corresponding ones in structure **A** (by −0.084 and +0.035 Å, respectively). The transition structute **TS_{AB}** (imaginary frequency 119.0*i* cm^{-1}) connects ion **A** with **B** and lies 10.9 kcal mol^{-1} above **A**. Also, the **A** → **B** rearrangement requires a substantial elongation of the C1−O bond distance, which increases up to 2.799 Å (**TS_{AB}**, Figure 1f). The transition structure **TS_S** (Figure 1g) refers to the resonant suprafacial H_2O shift from C1 to C3 of ion **A**. However, Table 4 indicates that this rearrangement is highly energy demanding, with a computed energy barrier of 24.2 kcal mol^{-1}, which approaches closely the dissociation enthalpy of ion **A** into $C_3H_5^+$ and H_2O (26 kcal mol^{-1}). This arises from the pronounced structural distortion in **TS_S**, relative to **A**, wherein the contribution of allylic resonance to the stabilization energy is strongly reduced by the unfavorable 180° → 169.6° variation of the H1−C1−C2−H3 dihedral angle. Angle distortion is accompanied by a pronounced variation of the C1−O bond distance, which changes from 1.575 to 2.968 Å. The observation that, in **TS_S**, the C1−O bond distance is much longer than the C2−O one (2.117 Å) suggests that water interacts mostly with the central C2 carbon of the allylic moiety. Finally, the transition structure for the resonant H_2O shift from C1 to C3 of ion **C** was located. This process occurs through the C_{2v}-symmetric structure **TS_C** (Figure 1h). The activation energy required for this degenerate rearrangement is as low as 1.6 kcal mol^{-1}, as reported in Table 4. This low energy barrier reflects the limited structural reorganization accompanying the **C** → **TS_C** transition, consisting essentially in the change of the H3−O bond distance from 2.433 to 1.994 Å.

Discussion

The Ionic Reagents. γ-Radiolysis of gaseous CH_4 and C_3H_8 produces known yields of $C_nH_5^+$ (n = 1, 2) ($G(C_nH_5^+)$ = 1.9 (n = 1); 0.9 (n = 2))[20a] and $sC_3H_7^+$ ($G(sC_3H_7^+)$ = 3),[20b−e] respectively. The large excess (over ca. 100:1) of the bulk gas over the n-type nucleophiles present in the mixtures favors collisional thermalization of the radiolytic ions before their attack on the substrates. Thermal CH_5^+ ($H_f°$ = 216 kcal mol^{-1}),[5] $C_2H_5^+$ ($H_f°$ = 216 kcal mol^{-1}),[5] and $sC_3H_7^+$ ($H_f°$ = 190.9 kcal mol^{-1})[5] are powerful Brønsted acids (PA(CH_4) = 131.6 kcal mol^{-1}; PA(C_2H_4) = 162.6 kcal mol^{-1}; PA(C_3H_6) = 179.5 kcal mol^{-1}).[5] In 720 Torr of pure CH_4 and at $T \leq$ 120 °C, the CH_5^+ ions are present predominantly (>80%) in the monosolvated [CH_5^+•CH_4] form ($H_f°$ = ca. 191 kcal mol^{-1}).[21] Under the same conditions, the $C_2H_5^+$ ions are instead mostly naked (>90%).[22a] In 720 Torr of pure C_3H_8 and at $T \leq$ 120 °C, the $sC_3H_7^+$ ions are present in the monosolvated [$sC_3H_7^+$•C_3H_8] form ($H_f°$ = ca. 152 kcal mol^{-1}).[22b] The [CH_5^+•CH_4] and $C_2H_5^+$ ions may readily protonate all n-type nucleophiles present in the mixtures, including H_2O (PA = 166.5 kcal mol^{-1}),[5] which is a major ubiquitous impurity of the reaction mixture, either initially introduced in the system together with its bulk components or formed from its radiolysis. On the contrary, the [$sC_3H_7^+$•C_3H_8] ions are unable to transfer a proton to H_2O, since the process is ca. 27 kcal mol^{-1} endothermic. The average stationary concentration of H_2O in the radiolytic systems is estimated of the order of ca. 0.3−0.6 mol % (*vide infra*). When the relatively minor concentrations of **1S** and $(MeO)_3PO$ (≤0.14 mol %) and the substantial diffusion rate of H_2O in the gaseous medium are taken into account, most of the $C_nH_5^+$(n = 1, 2) ions generated in the CH_4 samples are able to attack H_2O producing predominantly H_3O^+ in yields approaching those of its $C_nH_5^+$-(n = 1, 2) precursors ($G(C_nH_5^+(n = 1, 2)) = 2.8$).[23] As mentioned before, the [$sC_3H_7^+$•C_3H_8] reactant, generated in the C_3H_8 systems, cannot protonate H_2O,[23] but it is able to alkylate

(20) (a) Ausloos, P.; Lias, S. G.; Gorden, R., Jr. *J. Chem. Phys.* **1963**, *39*, 3341. (b) Ausloos, P.; Lias, S. G. *J. Chem. Phys.* **1962**, *36*, 3163. (c) Lias, S. G.; Ausloos, P. *J. Chem. Phys.* **1962**, *37*, 877. (d) Sandoval, I. B.; Ausloos, P. *J. Chem. Phys.* **1963**, *38*, 2452. (e) Freeman, G. R. *Radiat. Res. Rev.* **1968**, *1*, 1.

(21) Hiraoka, K.; Kebarle, P. *J. Am. Chem. Soc.* **1975**, *97*, 4179.

(22) (a) Hiraoka, K.; Mori, T.; Yamabe, S. *Chem. Phys. Lett.* **1993**, *207*, 178. (b) Sunner, J. A.; Hirao, K.; Kebarle, P. *J. Phys. Chem.* **1989**, *93*, 4010.

(23) In methane, the [CH_5^+•CH_4] and $C_2H_5^+$ and, in propane, [$sC_3H_7^+$•C_3H_8] ions may attack the H_2O impurity yielding H_3O^+, C_2H_5-OH_2^+, and $sC_3H_7OH_2^+$. In the 40−120 °C temperature range and in the presence of several Torrs of H_2O, these ion may be present in multisolvated forms, e.g. [H_3O^+•$(H_2O)_3$] (cf.: Lau, Y. K.; Ikuta, S.; Kebarle, P. *J. Am. Chem. Soc.* **1982**, *104*, 1462). All of these ions are able to protonate **1S** (ref 24). Extensive ion clustering does not appreciably affect the estimate of the kinetic results of Table 5 and of the corresponding activation parameters. For instance, with [H_3O^+•$(H_2O)_3$] as the protonating agent, treatment of the experimental results of Tables 1−3, as described in the text, leads to log k_B = (11.4 ± 0.4) − [(7.3 ± 0.5) × 10^3]/2.303RT (correlation coeff = 0.965) and log k_C = (12.4 ± 0.5) − [(8.7 ± 0.6) × 10^3]/2.303RT (correlation coeff = 0.964). Essentially the same activation parameters are obtained by considering bare H_3O^+ or [$sC_3H_7^+$•C_3H_8] as the Brønsted acid catalyst (see text).

it and to protonate and alkylate all of the other stronger nucleophiles present.[24] Exothermic protonation may take place on either the oxygen atom of **1S**, yielding **IS**, or on its π-bond (with $C_nH_5^+(n = 1, 2)$), producing a 3-hydroxyhexan-4-yl cation.[24] The first process by far kinetically predominates, as testified by the absence of isomeric hexanones among the radiolytic products of Table 1. Their O-protonated forms are, in fact, the most stable structures which the hypothetical 3-hydroxyhexan-4-yl cation, if formed, would isomerize to via a very fast 1,2-hydrogen shift.[25] While undergoing quenching by multiple collisions with the bulk gas, oxonium intermediate **IS** may rearrange to its isomeric structures **IR** and **IIS-IIR** (but apparently not to the **IIIS-IIIR** ones) or lose the H_2O moiety yielding the corresponding 1-methyl-3-ethylallyl cations.

Since we are interested in investigating the gas phase intramolecular racemization and isomerization reactions in the oxonium intermediate **IS** (path iv of Scheme 1), it is crucial to recognize unequivocally the origin of radiolytic products, whether formed from **IS** (path iv of Scheme 1; R = Me, R′ = Et) or from 1-methyl-3-ethylallyl cations (path iii of Scheme 1), and to determine the relative contribution of these two processes to their yield. Besides, any conceivable role of the H_2O moiety, released by H_3O^+-protonation of **1S** in the CH_4 systems, in the conversion of **IS** to the final products must be assessed (paths i and ii of Scheme 1; NuH = H_2O).

Nature of the Radiolytic Products. The conditions used in the radiolytic experiments, in particular the very limited concentration of **1S** ($\leq$0.14 mol %) diluted in a large excess of the bulk gas, rule out direct radiolysis of the starting allylic alcohol as a significant route to the products of Table 1. Their exclusive ionic origin is ensured by the presence in the mixtures of an efficient radical scavenger (i.e., O_2 (ca. 0.5 mol %) and testified by the disappearance of the alcoholic **1R** and **2S-2R** products and by the exclusive formation of isomeric hexadienes, by adding 0.2 mol % of a powerful base, such as NEt_3 (PA = 232.3 kcal mol^{-1})[5] to the gaseous system.

As already pointed out, kinetic investigation of the gas phase intramolecular racemization and isomerization reactions in the oxonium intermediate **IS** (path iv of Scheme 1) requires unequivocal determination of (a) the attainment of thermal equilibration between the gaseous medium and the oxonium intermediate **IS** before its rearrangement, (b) the role of the H_2O moiety, arising from O-protonation of **1S** by H_3O^+ in the CH_4 systems, in the **IS** racemization and isomerization (paths i and ii of Scheme 1; NuH = H_2O), and (c) the origin of radiolytic products, whether formed from **IS** (path iv of Scheme 1; R = Me, R′ = Et) or from 1-methyl-3-ethylallyl cations (path iii of Scheme 1), and the evaluation of the relative contribution of these two processes to their yield.

Concerning the first two points, the observation that the yield and distribution of the **1R**, **2S**, and **2R** products obtained from protonation of **1S** in C_3H_8, where formation of H_3O^+ is thermochemically prevented, are fully comparable to those formed from the same process in CH_4, where H_3O^+ is the major acid catalyst (Table 1), provides strong evidence against any conceivable role of the H_2O moiety generated in methane from protonation of **1S** by H_3O^+ in the **IS** → **IR**, **IIS**, and **IIR** conversion (paths i and ii in Scheme 1, NuH = H_2O).[26] In addition, the same observation indicates that the extent of racemization and isomerization of **IS** depend neither on the exothermicity of O-protonation of **1S** nor on the cooling efficiency of the bulk gas but only on the temperature of the gaseous systems. This corroborates the hypothesis of rapid quenching of the **IS** intermediates, excited by the exothermicity of their formation processes, by multiple unreactive collisions with the bulk gas well before their rearrangement.

In the intramolecular rearrangement of **IS** (path iv of Scheme 1), no interchange between the moving H_2O and the external H_2O is expected. Therefore, having ruled out paths i and ii of Scheme 1 (NuH = H_2O) as being involved in the **IS** racemization and regioisomerization, recovery of the labeled **1S-1R** and **2S-2R** products from the **1S**/$H_2{}^{18}O$ systems (Table 3) can be only accounted for by partial dissociation of excited **IS** to give the free 1-methyl-3-ethylallyl cation and a H_2O molecule (path iii of Scheme 1), which will mix with $H_2{}^{18}O$ present in the bulk gas. Free 1-methyl-3-ethylallyl cations eventually react with all of the nucleophiles present in the mixture, including the $H_2{}^{18}O$ itself, producing a [**1S-1R**]/[**2S-2R**] = 1 mixture in decreasing yield by increasing the reaction temperature from 40 to 100 °C (Table 2). The $^{18}O/^{16}O$ distribution in the allylic products (=1.2 ± 0.1 (CH_4), 0.6 ± 0.1 (C_3H_8); Table 2)) reflects approximately the $[H_2{}^{18}O]/[H_2{}^{16}O]$ ratio in the corresponding irradiated mixtures. This means that the average content of water impurity in the irradiated mixtures ranges around 2−4 Torr (i.e., 0.3−0.6 mol %).

The low degree of ^{18}O-incorporation in the **1S-1R** and **2S-2R** products recovered in the **1S**/$H_2{}^{18}O$ systems (Table 3), as compared to that of the corresponding products from attack of free 1-methyl-3-ethylallyl cations on $H_2{}^{18}O$ (Table 2), indicates that both paths iii and iv of Scheme 1 concur to their formation. Path iii is expected to lead to **1S-1R** and **2S-2R** with significant ^{18}O-content (i.e., 54 ± 2% (CH_4) and 38 ± 3% (C_3H_8) (Table 2)). Path iv is expected to yield the same products but with no incorporation of the ^{18}O-label. Accordingly, the fraction ϕ(M) factor of the **1R** and **2S-2R** products of Table 1 arising from addition of free *exo*-1-methyl-*exo*-3-ethylallyl cations to H_2O (path iii in Scheme 1, NuH = H_2O)[27] present as an ubiquitous impurity in the radiolytic mixtures can be calculated from the ratio between their ^{18}O-content measured independently from protonation of **1S** in the presence of $H_2{}^{18}O$ (Table 3)[27] and that measured from protonation of 2,4-hexadienes under the same conditions (Table 2). The remaining fraction 1 − ϕ(M) comes

(24) Exact determination of the thermochemistry of these processes is presently inaccessible, owing to the lack of experimental thermochemical data for the ionic species involved. An approximate estimate of the PA of **1S** (ca. 204 kcal mol^{-1}) can be obtained from a correlation between the ionization energies and the proton affinities of alcohols (ref 5). The heat of formation of the 3-hydroxyhexan-4-yl cation (ca. 140 kcal mol^{-1}) is estimated by means of a modified isodesmic substitution (ref 25). This leads to a site PA value for the π-bond of **1S** of ca. 176 kcal mol^{-1}. Accordingly, the exothermicity of protonation at the oxygen atom of **1S** by ROH_2^+ (R = H, C_2H_5, and sC_3H_7) would be around 39, 16, and 13 kcal mol^{-1}, respectively. The same process from $[sC_3H_7^+ \bullet C_3H_8]$ is exothermic by 10 kcal mol^{-1}. Protonation of the π-bond of **1S** by H_3O^+ is 11 kcal mol^{-1} exothermic. The same process by $[sC_3H_7^+ \bullet C_3H_8]$, $C_2H_5OH_2^+$, or $sC_3H_7OH_2^+$ is endothermic by 18, 12, and 15 kcal mol^{-1}, respectively.

(25) Bowen, R. D.; Williams, D. H. *J. Am. Chem. Soc.* **1978**, *100*, 7454.

(26) Further pieces of evidence against occurence of the bimolecular paths i and ii of Scheme 1 (NuH = $H_2{}^{18}O$, Table 3), arise from (a) the [^{18}O-**1R**]/[^{18}O-**2S-2R**] yield ratios, calculated from Table 3 (=0.58 ± 0.11 (CH_4), 0.51 ± 0.07 (C_3H_8)), which coincide within the uncertainty range with those from Table 2 (=0.50 ± 0.02 (CH_4), 0.45 ± 0.02 (C_3H_8)) (ref 27); (b) the absolute yields of products of Table 3 and their ^{18}O-content which do not exhibit any monotonic increase with temperature, as would be expected if bimolecular nucleophilic displacements i and ii were responsible for their formation; and (c) the absence of any appreciable occurrence of the quasi-resonant bimolecular $H_2{}^{18}O$-to-$H_2{}^{16}O$ displacement in closely related allylic alcohols (i.e., O-protonated 1-buten-3-ol and isomeric 2-buten-1-ols (ref 2).

(27) This is true as far as the hypothetical bimolecular pathways generate, in the **1S**/$H_2{}^{18}O$ systems, unbalanced yields of ^{18}O-labeled **1S-1R** and **2S-2R** products. Otherwise, the occurrence and the extent of conceivable bimolecular pathways cannot be discriminated from the unimolecular pathway iii on the simple basis of the ^{18}O-content in the radiolytic products. Yet, in this latter special case, the fraction ϕ(M) of **1R** and **2S-2R** products of Table 1, calculated from the ratio between their ^{18}O-content from Tables 3 and 2 (see further in the text) does still express the relative efficiency of processes other than the intramolecular rearrangement iv of **IS** (Scheme 1), irrespective of whether they are unimolecular (path iii) or bimolecular (paths i and ii) in character.

Table 5. Rate Constants of Intramolecular Racemization and Isomerization of **IS**

bulk gas	reactn temp (°C)	reactn extent[a]		reactn time[b] t_{reactn} ($\times 10^8$ s)	rate constants (10^{-6} s^{-1})			
		Y_{1R}	Y_{2R-2S}		k_{1R}[c]	k_{2R-2S}[c]	k_C[d]	k_B[e]
CH_4	40	0.040	0.028	2.9	1.4	1.0	1.9 (6.27)	2.0 (6.29)
CH_4	70	0.173	0.099	2.0	9.5	5.2	14.2 (7.15)	11.0 (7.04)
CH_4	100	0.271	0.158	2.3	13.8	7.5	21.1 (7.32)	16.5 (7.25)
CH_4	120	0.394	0.207	2.3	21.3	9.9	37.0 (7.57)	22.7 (7.36)
C_3H_8	40	0.043	0.029	2.5	1.8	1.2	2.4 (6.38)	2.4 (6.38)
C_3H_8	100	0.346	0.203	3.0	14.0	7.5	22.2 (7.34)	17.2 (7.23)

[a] Reaction extent, Y_M, expressed by $G(M)(1 - \phi)/G°$ (see text). [b] Reaction time, t_{reactn}, calculated from the reciprocal of the first-order collision constant between **IS** and $(MeO)_3PO$ (see text). [c] $k = t_{reactn}^{-1} \ln(1 - Y_M)^{-1}$ (see text). [d] $k_C = t_{reactn}^{-1} \ln[1 - 2(Y_{1R} - 0.5Y_{2R-2S})]^{-1}$ (see text), log k_C in parentheses. [e] $k_B = t_{reactn}^{-1} \ln(1 - 2Y_{2R-2S})^{-1}$ (see text), log k_B in parentheses.

from intramolecular rearrangement of **IS** (path iv of Scheme 1; R = Me, R′ = Et). On the basis of this information, the yield of the **1R** and **2S-2R** alcohols of Table 1 actually arising from intramolecular H_2O shifts in the collisionally stabilized **IS** intermediates (path iv in Scheme 1) can be estimated from the corresponding $G(M)(1 - \phi(M))$ products.

Under the experimental conditions of Table 1, the extent of the acid-catalyzed **IS** → **IR** racemization and **IS** → **IIS-IIR** regioisomerization can be expressed as the ratio Y_M between the corresponding $G(M)(1 - \phi(M))$ factor and the $G°$ terms, defined as number of protonating species formed by absorption of 100 eV energy, which is able to generate stable **IS** intermediates by O-protonation of **1S**. Within the plausible hypothesis that the exothermic attack on **1S** and B(=$(MeO)_3PO$) by the protonating species is very efficient and totally unselective, $G°$ can be adequately expressed by the following equation

$$G° = \{[G(\text{protonating species})k_1[\mathbf{1S}]]/[(k_1[\mathbf{1S}] + k_2[B]]\} - G(\text{dienes}) - G(\text{ethers}) \quad (1)$$

where G(protonating species) is taken as equal to either $G(H_3O^+) \cong G(C_nH_5^+(n = 1, 2)) = 2.8$[23] for the methane systems or $G(sC_3H_7^+) = 3$[20b−e] for the propane systems, G(dienes)[28] represents the overall absolute yield of the isomeric hexadienes formed in the irradiated mixtures, G(ethers) is the combined absolute yield of *trans*-3-isopropoxy-4-hexenes and *trans*-2-isopropoxy-3-hexenes produced in the propane samples (Table 1), and k_1 and k_2 are the collision rate constants of the protonating catalyst toward **1S** and B(=$(MeO)_3PO$), respectively, estimated at any given temperature by using the trajectory calculation method.[29]

When it is taken into account that exothermic proton transfer from gaseous Brønsted acids, including the oxonium ions of Scheme 2, to powerful bases, such as $(MeO)_3PO$, is generally fast, the first-order rate constants for the formation of **1R** (k_{1R}) and **2S-2R** (k_{2S-2R}) at any given temperature can be expressed by $k_{1R} = t_{reactn}^{-1} \ln(1 - Y_{1R})^{-1}$ and $k_{2S-2R} = t_{reactn}^{-1} \ln(1 - Y_{2S-2R})^{-1}$, with t_{reactn} corresponding to the collision interval of **IS** with the base B[30] under the assumption that the trapping reaction occurs with unit efficiency. The relevant results are listed in Table 5.

Derivation of the activation parameters for intramolecular racemization and isomerization of **IS** from the data of Table 5 requires adequate modeling of the individual rearrangement processes.

The Regioisomerization and Racemization Model. Comparison between the [**1S-1R**]/[**2S-2R**] ≈ 1 distribution from addition of free *exo*-1-methyl-*exo*-3-ethylallyl cations on external H_2O molecules and that (i.e., [**1S-1R**]/[**2S-2R**] = 2.3−3.8) from protonation of **1S** (Table 1) excludes that, at any temperature, the two pathways involve the same intermediate, namely a loosely bound complex between 1-methyl-3-ethylallyl cations and H_2O. Modeling of the gas phase intramolecular **IS** → **IR** racemization and **IS** → **IIR-IIS** isomerization necessarily implies the intervention of tightly bound reaction complexes, wherein the migrating H_2O and the delocalized π-system of the allylic residue become orthogonal. In the tightly bound symmetric intermediate involved in the **IS** → **IR** racemization, equal is the probability that the H_2O moiety rebonds to the original side of the orbital (internal return to **IS**) or moves to the other side, yielding the enantiomer **IR**. In the tightly bound symmetric intermediate involved in the **IS** → **IIR-IIS** regioisomerization, rebonding of H_2O to the allylic carbons would yield both the **IS-IR** and **IIS-IIR** racemates in proportions depending on the corresponding activation free energies. Alternative hypothesis for intramolecular isomerization, such as that based on the complete racemization of the starting **IS** to **IS-IR** followed by the slow **IS-IR** → **IIS-IIR** regioisomerization, contrasts with the limited racemization (Y_{1R}; Table 5) and isomerization yield factors (Y_{2R-2S}; Table 5) measured under all experimental conditions and with the observed increase of their ratio with temperature.[31]

The intermediacy of tightly bound structured complexes in intramolecular **IS** racemization and isomerization finds further support in the *ab initio* theoretical analysis of the critical structures of the model [$C_3H_5^+/H_2O$] system (Figure 1). Here, the transition structure **TS$_{AB}$** separates the starting oxonium ion **A** from ion **B**, wherein the H_2O moiety is located in the plane of the allyl cation between H1 and H5. The transition structure **TS$_{AC}$** connects instead isomer **A** with ion **C**, wherein the H_2O moiety lies again in the same plane but between H2 and H3 of the allylic moiety. The latter structure is separated from the degenerate one, wherein H_2O is placed between H3 and H4 (denoted as **C′**), by the symmetric transition structure **TS$_C$** lying slightly above **TS$_{AC}$**. Therefore, in the unimolecular rearrangement of O-protonated allyl alcohol depicted in Scheme 3, structure **B** governs both its resonant isomerization, when the

(28) The isomeric hexadienes of Table 1 may as well arise in part from $(MeO)_3PO$-induced bimolecular E2 and E2′ elimination in **IS** or in its ionic isomers. However, the conceivable interference from these bimolecular elimination processes does not affect the estimate of the rate constants of Table 5, provided that they occur to the same extent irrespective of the specific isomer (cf., ref 3c). In this case, in fact, occurrence of bimolecular E2 and E2′ eliminations may affect the absolute yields of the racemization and isomerization products, but not their relative distribution.

(29) Valves for 10^9k_1 in cm^3 $molecule^{-1}$ s^{-1} (acid catalyst; temperature in °C): 2.84 (H_3O^+; 40); 2.70 (H_3O^+; 70); 2.58 (H_3O^+; 100); 2.51 (H_3O^+; 120); 1.66 ([$sC_3H_7^+$•C_3H_8]; 40); 1.51 ([$sC_3H_7^+$•C_3H_8]; 100). Valves for 10^9k_2 in cm^3 $molecule^{-1}$ s^{-1} (acid catalyst; temperature in °C) 3.97 (H_3O^+; 40); 3.84 (H_3O^+; 70); 3.72 (H_3O^+; 100); 3.67 (H_3O^+; 120); 2.21 ([$sC_3H_7^+$•C_3H_8]; 40); 2.08 ([$sC_3H_7^+$•C_3H_8]; 100); Su, T.; Chesnavitch, W. J. *J. Chem. Phys.* **1982**, *76*, 5183.

(30) The reaction time, t_{reactn}, is taken as the inverse of the first-order collision rate constant $k = k_3[(MeO)_3PO]$ between **IS** and the $(MeO)_3PO$ base, with the collision rate constant k_3 calculated according to ref 29 (10^9k_3 cm^3 $molecule^{-1}$ s^{-1} (temperature in °C) = 2.11 (40); 2.05 (70); 1.99 (100); 1.96 (120)).

(31) The same trend, coupled with the substantial activation barrier expected for the suprafacial 1,3-shift of H_2O in **IS** (24.2 kcal mol^{-1} in the model [$C_3H_5^+$,H_2O] system), excludes the possibility of slow isomerization of the starting **IS** to **IIR**, followed by fast **IIR** → **IIS** racemization.

Scheme 3

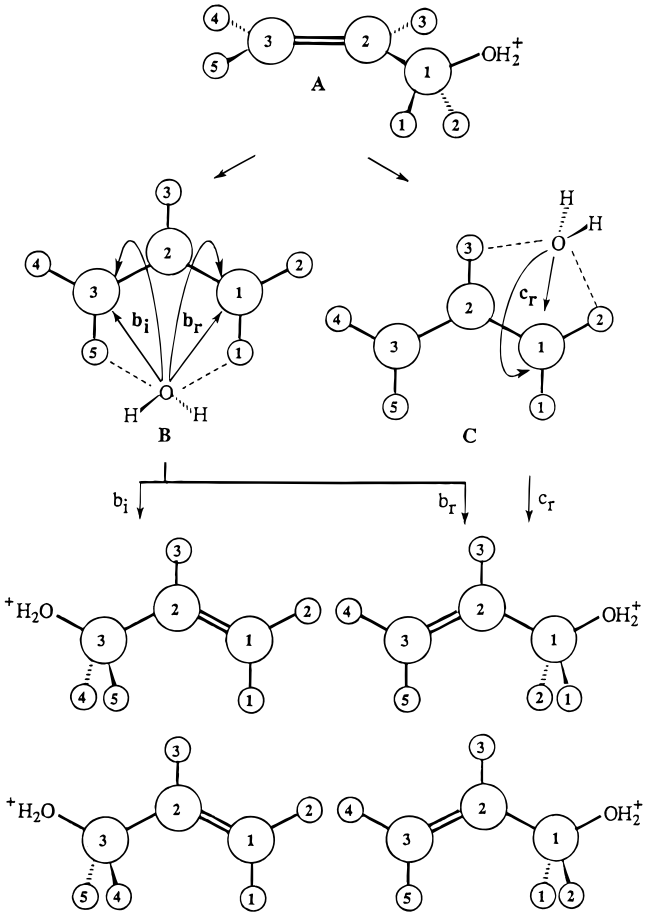

Scheme 4

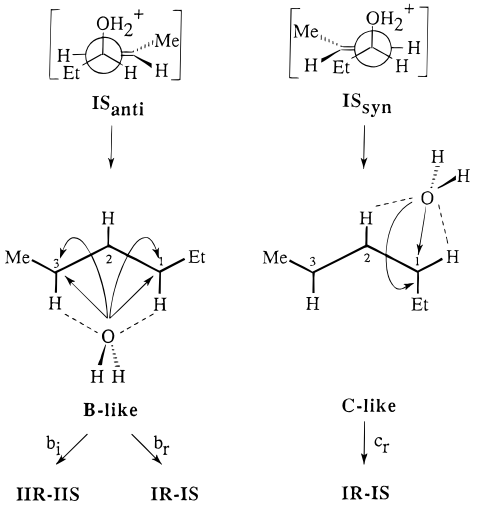

H_2O moiety moves to both sides of the C3 one (route b_i in Scheme 3), and racemization, when the H_2O moiety internally returns to both sides of the C1 carbon (route b_r in Scheme 3). Concerning structure **C**, it may evolve either to **C′** via $\mathbf{TS_C}$ or to **A** via $\mathbf{TS_{AC}}$ (route c_r in Scheme 3). The uncertainty (≥2%) in the theoretical approaches used to describe $\mathbf{TS_C}$ and $\mathbf{TS_{AC}}$ does not allow to predict the most favored **C** isomerization pathway whether $\mathbf{C \rightarrow TS_C \rightarrow C'}$ or $\mathbf{C \rightarrow TS_{AC} \rightarrow A}$. However, in the **C**-like structure of **IS** (Scheme 4), the presence of a methyl group on the *cis*-C3 position adjacent to the C2−H bond inhibits the hypothetical formation of a hydrogen-bonded **C′**-like structure.[32] As a consequence, the conceivable $\mathbf{C \leftrightarrow TS_C \leftrightarrow C'}$-like equilibrium in **IS** would be strongly shifted on the left side, thus making the $\mathbf{C \rightarrow TS_{AC} \rightarrow A}$ racemization pathway

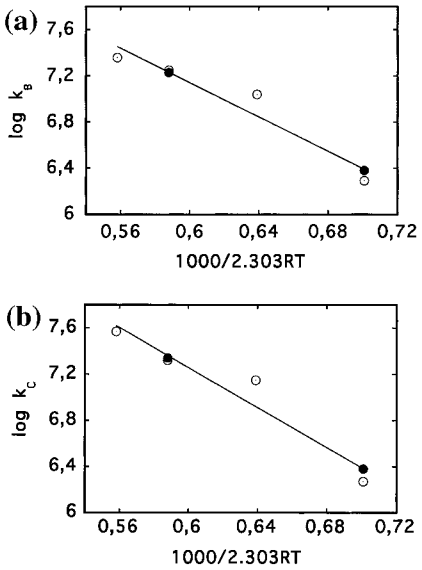

Figure 2. Arrhenius plots for the **IS** → **B**-like (a) and **IS** → **C**-like (b) intramolecular rearrangements in 720 Torr of methane (open circles) or propane (solid circles).

the only accessible rearrangement path open to **C**. Thus, the racemization route c_r of Scheme 3 is the preferred pathway open to structure **C**.

Therefore, the structured complexes governing rearrangement in **IS** are those depicted in Scheme 4, namely **B**-like and **C**-like. The **IS** → **IIR-IIS** isomerization is controlled only by the **B**-like structure (route b_i), whereas the **IS** → **IR-IS** racemization is governed by both the **B**-like (route b_r) and the **C**-like structures (route c_r).

Treatment of the Y_M factors of Table 5 to derive the activation parameters governing **IS** unimolecular rearrangements requires an estimate of the relative contribution of pathways b_r and c_r of Scheme 4 to the yield of racemization product **1R** ($Y_{\mathbf{1R}}$ in Table 5). A way is to consider the [**1S-1R**]/[**2S-2R**] ≈ 1 distribution from addition of free *exo*-1-methyl-*exo*-3-ethylallyl cations to H_2O as evidence of essentially equal stability for their oxonium precursors **IS-IR** and **IIR-IIS**. Thereby, following the Hammond postulate, approximately equal free energy activation barriers can be expected for the conversion of **B**-like (Scheme 4) into the more stable **IR-IS** and **IIR-IIS** intermediates. Along this line, the contribution of route b_r of Scheme 4 to the **IS** → **IR** process is taken equal to one-half of the combined **2S-2R** isomerization yield (i.e., $0.5Y_{\mathbf{2R-2S}}$). Obviously, the contribution of route c_r of Scheme 4 to the **IS** → **IR** process is calculated from $Y_{\mathbf{1R}} - 0.5Y_{\mathbf{2R-2S}}$. As a consequence, the formation rate of the **B**-like (Scheme 4) structure can be expressed by $k_B = t_{\text{reactn}}^{-1} \ln(1 - 2Y_{\mathbf{2R-2S}})^{-1}$. Similarly, considering equal the probability of conversion of the **C**-like structure (Scheme 4) to the **IR** and **IS** (internal return) enantiomers, the formation rate of the **C**-like structure is expressed by $k_C = t_{\text{reactn}}^{-1} \ln[1 - 2(Y_{\mathbf{1R}} - 0.5Y_{\mathbf{2R-2S}})]^{-1}$. The values of the k_B and k_C rate constants, obtained in the 40−120 °C range, are listed in Table 5. The corresponding Arrhenius plots are shown in Figure 2. The observation that the k_B and k_C rate constants from the propane systems at 40 and 100 °C fit the Arrhenius correlation obtained from the methane samples demonstrates that the kinetics of the gas phase **IS** racemization and regioisomerization are independent of the nature and the strength of the Brønsted acid catalyst, whether H_3O^+ or $[sC_3H_7^+ \cdot C_3H_8]$, and of the heat capacity of

(32) Kebarle and co-workers (Hiraoka, K.; Grimsrud, E. P.; Kebarle, P. *J. Am. Chem. Soc.* **1974**, *96*, 3359) demonstrated that replacement of a H atom by an alkyl group in an oxonium ion prevents hydrogen bonding on that position by n-type molecules and, thus, the buildup of the corresponding cluster.

the bulk gas. This implies that **IS** racemization and regioisomerization kinetics are only temperature-dependent and that the oxonium intermediate **IS** is in thermal equilibrium with the bath gas well before its racemization and regioisomerization. In addition, the same observation confirms the previous indications that the H_2O moiety arising from proton transfer from H_3O^+ to **1S** does not play any appreciable kinetic and mechanistic role in the **IS** rearrangement in the methane systems. Regression analysis of all the data of Figure 2a leads to the equation $\log k_B = (11.6 \pm 0.4) - [(7.4 \pm 0.5) \times 10^3]/2.303RT$, with a correlation coefficient of 0.975. The same procedure applied to the data of Figure 2b leads to the equation $\log k_C = (12.4 \pm 0.5) - [(8.6 \pm 0.6) \times 10^3]/2.303RT$, with a correlation coefficient of 0.976.[23]

The difference between the experimental activation energy barriers for the **IS** → **C**-like and the **IS** → **B**-like rearrangements ($E_C^{\ddagger} - E_B^{\ddagger} = (8.6 \pm 0.6) - (7.4 \pm 0.5) = 1.2 \pm 1.1$ kcal mol^{-1}) compares well with the energy gap between the transition structures $\mathbf{TS_{AC}}$ and $\mathbf{TS_{AB}}$ ($11.8 - 10.9 = 0.9$ kcal mol^{-1}) computed for the [$C_3H_5^+/H_2O$] system (Table 4). The lower absolute values of the energy barriers for the **IS** intramolecular rearrangements parallel the expectedly lower C−O bond energy in **IS**, relative to O-protonated allyl alcohol.

Conformational Effects. On the basis of the above models, the dynamics of the gas phase rearrangement of **IS** depends upon the specific structure (**B**-like vs **C**-like in Scheme 4) involved in the reaction coordinate, which in turn is determined by the particular conformation of the starting oxonium intermediate. *Ab initio* conformational analysis of O-protonated allyl alcohol indicates that the most stable of its rotamers are those with the C−O bond coplanar with the π-bond of the allyl moiety, where p-π conjugative stabilization and charge delocalization between the H_2O moiety and the allyl cation skeleton are maximized. In fact, the transition structure with the C−O bond orthogonal to the π-bond of the allyl moiety is found to lie ca. 30 kcal mol^{-1} above the most stable coplanar conformation. It follows that radiolytic protonation of **1S** leads essentially to two non-interconverting conformers of **IS**, namely $\mathbf{IS_{syn}}$, where the double bond is *syn* to the ethyl group, and $\mathbf{IS_{anti}}$, where the double bond is *anti* to the ethyl group (Scheme 4), in proportions reflecting the relative population of the corresponding **1S** rotamers in their encounter complexes with the protonating agent. In $\mathbf{IS_{syn}}$, the quasi-coplanar hydrogens are H2 and H3, and thus, the **C**-like structure governs the intramolecular H_2O shift. In $\mathbf{IS_{anti}}$, instead, the quasi-coplanar hydrogens are H1 and H5, and thus, the **B**-like structure governs the intramolecular H_2O motion. In other words, $\mathbf{IS_{syn}}$ follows exclusively the racemization path c_r of Scheme 4, whereas two rearrangement channels are open to $\mathbf{IS_{anti}}$, namely the isomerization path b_i and racemization path b_r of Scheme 4. According to the **B**-like structure, the isomerization path b_i would generate exclusively the *trans*-isomers **IIR**-**IIS** and not the *cis* ones **IIIR**-**IIIS**, as actually confirmed by the experimental results (Table 1). This coincidence is somewhat reassuring on the soundness of the rearrangement models adopted.

Further support is obtained from inspection of the activation parameters inferred from the Arrhenius plots of Figure 2. Indeed, the measured 1.2 ± 1.1 kcal mol^{-1} difference between the activation energy of the $\mathbf{IS_{syn}}$ → **C**-like and the $\mathbf{IS_{anti}}$ → **B**-like rearrangements reflects the difference between the energy gap of the relevant transition structures and that of the $\mathbf{IS_{syn}}$ and $\mathbf{IS_{anti}}$ pair. In view of the expected stability trend $\mathbf{IS_{syn}} < \mathbf{IS_{anti}}$, the 1.2 ± 1.1 kcal mol^{-1} activation energy difference conforms to the ca. 3 kcal mol^{-1} stability gap between *exo*-1-methyl-*exo*-3-ethylallyl cation and *exo*-1-methyl-*endo*-3-ethylallyl cation, estimated on the basis of *ab initio* calculations on strictly related systems.[33] This points to transition structures for the $\mathbf{IS_{syn}}$ → **C**-like and $\mathbf{IS_{anti}}$ → **B**-like processes wherein a substantial fraction of the positive charge is delocalized over the allyl moiety.

Comparison with Solution Chemistry Studies. Demonstration of the occurrence of the intimate **B**-like and **C**-like ion−dipole structures in the gas phase provides further insight into the occurrence and the role of ion−molecule pairs in acid-catalyzed racemization and isomerization of optically active alcohols, including allylic alcohols,[34] in solution.[6−12] In the elucidation of this mechanism, the rates of ^{18}O exchange in water of labeled alcohols (or in $H_2{}^{18}O$ of unlabeled alcohols) of suitable structure were compared with the rates of loss of optical activity and of various competing rearrangements.[6−9] Within the hypothesis of a pure unimolecular mechanism for racemization and isomerization, the kinetic data can be accommodated by a reaction pattern involving the intermediacy of intimate ion−molecule pairs where the departing water does not equilibrate immediately with the solvent but remains closely associated with the carbocation.[10−12] In this way, the leaving water has a greater chance of being recaptured by the carbocation than the water molecules from the bulk of the solution. However, the premises on which this model is based are weakened by the observation that the rates at which the leaving moiety moves within the solvation sphere around the carbocation skeleton or equilibrates with the bulk solvent depend on the relative lifetimes of the carbocation and of its solvent shell which, in turn, depend on the structure of the carbon skeleton[6−12] and the nature of the solvent and of the leaving moiety.[13−15] Unfortunately, these same factors may influence the reaction mechanism itself, so that the incursion of a bimolecular S_N2 pathway and of dehydration−rehydration processes to the formation of the racemization and exchange products cannot be completely excluded.[11−12,34]

The important role of ion−neutral complex in gas phase ion chemistry and the strict analogies to ion−molecule pairs in solution is now well recognized.[35] After careful evaluation of the contribution of free allyl ions to the formation of the racemization and isomerization products, the present gas phase study demonstrates that, in a model O-protonated chiral allylic alcohol, the leaving H_2O moiety does not readily interchange with external H_2O molecules (including the conjugate base of the H_3O^+ acid catalyst), but rather moves intramolecularly around the allyl cation backbone producing eventually the racemization and regioisomerization products. Unlike solution studies, this intramolecular pattern is discernible in the gas phase, owing to the absence of bulk H_2O solvent around the oxonium ion and, therefore, of a rapid interchange of the moving moiety with the reaction medium. In agreement with previous circumstantial evidence obtained in solution,[6−12] the dynamics of the gas phase racemization and isomerization reactions is governed by the occurrence and the relative stability of structured ion−neutral complexes (i.e., **B**-like and **C**-like), with the moving H_2O electrostatically coordinated to the in-plane hydrogens of the allylic moiety. A significant role in determining the formation of these structured intermediates is played by conformational factors in their oxonium precursors ($\mathbf{IS_{syn}}$ vs $\mathbf{IS_{anti}}$). A similar role, which is expected to be operative in any media, has not been detected in solution yet.

Acknowledgment. This research was supported by the Italian Ministero dell'Università e della Ricerca Scientifica e Tecnologica (MURST). We thank F. Cacace for his continuous encouragement and pertinent suggestions.

JA960212P

(33) Mayr, H.; Forner, W.; Schleyer, P. v. R. *J. Am. Chem. Soc.* **1979**, *101*, 6031.
(34) Young, W. G.; Franklin, J. S. *J. Am. Chem. Soc.* **1966**, *88*, 785.
(35) McAdoo, D. J.; Morton, T. H. *Acc. Chem. Res.* **1993**, *26*, 295.